Measurements of J/ψ decays into $\omega K\bar{K}\pi$, $\phi K\bar{K}\pi$ and $\eta K^0_S K^{\pm}\pi^{\mp}$

M. Ablikim[1], J. Z. Bai[1], Y. Bai[1], Y. Ban[11], X. Cai[1], H. F. Chen[16], H. S. Chen[1], H. X. Chen[1], J. C. Chen[1], Jin Chen[1], X. D. Chen[5], Y. B. Chen[1], Y. P. Chu[1], Y. S. Dai[18], Z. Y. Deng[1], S. X. Du[1], J. Fang[1], C. D. Fu[14], C. S. Gao[1], Y. N. Gao[14], S. D. Gu[1], Y. T. Gu[4], Y. N. Guo[1], Z. J. Guo[15a], F. A. Harris[15], K. L. He[1], M. He[12], Y. K. Heng[1], J. Hou[10], H. M. Hu[1], T. Hu[1], G. S. Huang[1b], X. T. Huang[12], Y. P. Huang[1], X. B. Ji[1], X. S. Jiang[1], J. B. Jiao[12], D. P. Jin[1], S. Jin[1], Y. F. Lai[1], H. B. Li[1], J. Li[1], R. Y. Li[1], W. D. Li[1], W. G. Li[1], X. L. Li[1], X. N. Li[1], X. Q. Li[10], Y. F. Liang[13], H. B. Liao[1c], B. J. Liu[1], C. X. Liu[1], Fang Liu[1], Feng Liu[6], H. H. Liu[1d], H. M. Liu[1], J. B. Liu[1e], J. P. Liu[17], H. B. Liu[4], J. Liu[1], Q. Liu[15], R. G. Liu[1], S. Liu[8], Z. A. Liu[1], F. Lu[1], G. R. Lu[5], J. G. Lu[1], C. L. Luo[9], F. C. Ma[8], H. L. Ma[2], L. L. Ma[1f], Q. M. Ma[1], M. Q. A. Malik[1], Z. P. Mao[1], X. H. Mo[1], J. Nie[1], S. L. Olsen[15], R. G. Ping[1], N. D. Qi[1], H. Qin[1], J. F. Qiu[1], G. Rong[1], X. D. Ruan[4], L. Y. Shan[1], L. Shang[1], C. P. Shen[15], D. L. Shen[1], X. Y. Shen[1], H. Y. Sheng[1], H. S. Sun[1], S. S. Sun[1], Y. Z. Sun[1], Z. J. Sun[1], X. Tang[1], J. P. Tian[14], G. L. Tong[1], G. S. Varner[15], X. Wan[1], L. Wang[1], L. L. Wang[1], L. S. Wang[1], P. Wang[1], P. L. Wang[1], W. F. Wang[1g], Y. F. Wang[1], Z. Wang[1], Z. Y. Wang[1], C. L. Wei[1], D. H. Wei[3], Y. Weng[1], N. Wu[1], X. M. Xia[1], X. X. Xie[1], G. F. Xu[1], X. P. Xu[6], Y. Xu[10], M. L. Yan[16], H. X. Yang[1], M. Yang[1], Y. X. Yang[3], M. H. Ye[2], Y. X. Ye[16], C. X. Yu[10], G. W. Yu[1], C. Z. Yuan[1], Y. Yuan[1], S. L. Zang[1h], Y. Zeng[7], B. X. Zhang[1], B. Y. Zhang[1], C. C. Zhang[1], D. H. Zhang[1], H. Q. Zhang[1], H. Y. Zhang[1], J. W. Zhang[1], J. Y. Zhang[1], X. Y. Zhang[12], Y. Y. Zhang[13], Z. X. Zhang[11], Z. P. Zhang[16], D. X. Zhao[1], J. W. Zhao[1], M. G. Zhao[1], P. P. Zhao[1], Z. G. Zhao[1i], H. Q. Zheng[11], J. P. Zheng[1], Z. P. Zheng[1], B. Zhong[9] L. Zhou[1], K. J. Zhu[1], Q. M. Zhu[1], X. W. Zhu[1], Y. C. Zhu[1], Y. S. Zhu[1], Z. A. Zhu[1], Z. L. Zhu[3], B. A. Zhuang[1], B. S. Zou[1]

(BES Collaboration)

[1] *Institute of High Energy Physics, Beijing 100049, People's Republic of China*
[2] *China Center for Advanced Science and Technology(CCAST), Beijing 100080, People's Republic of China*
[3] *Guangxi Normal University, Guilin 541004, People's Republic of China*
[4] *Guangxi University, Nanning 530004, People's Republic of China*
[5] *Henan Normal University, Xinxiang 453002, People's Republic of China*
[6] *Huazhong Normal University, Wuhan 430079, People's Republic of China*
[7] *Hunan University, Changsha 410082, People's Republic of China*
[8] *Liaoning University, Shenyang 110036, People's Republic of China*
[9] *Nanjing Normal University, Nanjing 210097, People's Republic of China*
[10] *Nankai University, Tianjin 300071, People's Republic of China*
[11] *Peking University, Beijing 100871, People's Republic of China*
[12] *Shandong University, Jinan 250100, People's Republic of China*
[13] *Sichuan University, Chengdu 610064, People's Republic of China*
[14] *Tsinghua University, Beijing 100084, People's Republic of China*
[15] *University of Hawaii, Honolulu, HI 96822, USA*
[16] *University of Science and Technology of China, Hefei 230026, People's Republic of China*

[17] *Wuhan University, Wuhan 430072, People's Republic of China*
[18] *Zhejiang University, Hangzhou 310028, People's Republic of China*

[a] *Current address: Johns Hopkins University, Baltimore, MD 21218, USA*
[b] *Current address: University of Oklahoma, Norman, Oklahoma 73019, USA*
[c] *Current address: DAPNIA/SPP Batiment 141, CEA Saclay, 91191, Gif sur Yvette Cedex, France*
[d] *Current address: Henan University of Science and Technology, Luoyang 471003, People's Republic of China*
[e] *Current address: CERN, CH-1211 Geneva 23, Switzerland*
[f] *Current address: University of Toronto, Toronto M5S 1A7, Canada*
[g] *Current address: Laboratoire de l'Accélérateur Linéaire, Orsay, F-91898, France*
[h] *Current address: University of Colorado, Boulder, CO 80309, USA*
[i] *Current address: University of Michigan, Ann Arbor, MI 48109, USA*

(Dated: February 2, 2008)

Abstract

The decays of $J/\psi \to \omega K\bar{K}\pi$ and $J/\psi \to \phi K\bar{K}\pi$ are studied using 5.8×10^7 J/ψ events collected with the Beijing Spectrometer (BESII) at the Beijing Electron-Positron Collider (BEPC). The $K^0_S K^\pm\pi^\mp$ and $K^+K^-\pi^0$ systems, produced in $J/\psi \to \omega K\bar{K}\pi$, have enhancements in the invariant mass distributions at around 1.44 GeV/c^2. However, there is no evidence for mass enhancements in the $K\bar{K}\pi$ system in $J/\psi \to \phi K\bar{K}\pi$. The branching fractions of $J/\psi \to \omega K^0_S K^\pm\pi^\mp$, $\phi K^0_S K^\pm\pi^\mp$, $\omega K^*\bar{K} + c.c.$, and $\phi K^*\bar{K} + c.c.$ are obtained, and the $J/\psi \to \eta K^0_S K^\pm\pi^\mp$ branching fraction is measured for the first time.

PACS numbers: 13.20.Gd, 13.25.Gv, 13.20.-v, 12.38.Qk, 14.40.-n

I. INTRODUCTION

A pseudoscalar gluonium candidate, the so-called $E/\iota(1440)$, was observed in $p\bar{p}$ annihilation in 1967 [1] and in J/ψ radiative decays in the 1980's [2, 3, 4]. After 1990, more and more observations revealed the existence of two resonant structures around 1.44 GeV/c^2 in $a_0(980)\pi$, $K\bar{K}\pi$, and $K^*\bar{K}$ spectra [5, 6, 7, 8, 9, 10, 11]. They showed that the lower state, $\eta(1405)$, has large couplings to $a_0(980)\pi$ and $K\bar{K}\pi$, while the high mass state, $\eta(1475)$, favors $K^*\bar{K}$. The $\eta(1405)$ was also confirmed by MarkIII [12], Crystal Barrel [13], and DM2 [4] in decays into $\eta\pi\pi$ in J/ψ radiative decays and $\bar{p}p$ annihilations.

In contrast, although $\eta(1475)$ was observed in $K\bar{K}\pi$ ($K^*\bar{K}$) [5, 6, 7, 8, 9, 10, 11], it was not seen in $\eta\pi\pi$. Nonetheless, the study of $K\bar{K}\pi$ and $\eta\pi\pi$ channels in $\gamma\gamma$ collisions [14] showed that $\eta(1475)$ appeared in $K\bar{K}\pi$, but not in $\eta\pi\pi$, while $\eta(1405)$ appeared in neither channel.

The study of the decays $J/\psi \to \{\gamma, \omega, \phi\}K\bar{K}\pi$ is a useful tool in the investigation of quark and possible gluonium content of the states around 1.44 GeV/c^2. In this paper, we investigate the possible structure in the $K\bar{K}\pi$ final state in J/ψ hadronic decays at around 1.44 GeV/c^2, and measure the branching fraction of $J/\psi \to \eta K^0_S K^\pm \pi^\mp$ for the first time, based on 5.8×10^7 J/ψ events collected with the Beijing Spectrometer at the Beijing Electron-Positron Collider (BEPC) .

II. THE BES DETECTOR

BESII is a large solid-angle magnetic spectrometer that is described in detail elsewhere [15]. Charged particle momenta are determined with a resolution of $\sigma_p/p = 1.78\%\sqrt{1+p^2}$ (p in GeV/c^2) in a 40-layer cylindrical main drift chamber (MDC). Particle identification (PID) is accomplished using specific ionization (dE/dx) measurement in the MDC and time-of-flight (TOF) information in a barrel-like array of 48 scintillation counters. The dE/dx resolution is $\sigma_{dE/dx} \simeq 8.0\%$; the TOF resolution is $\sigma_{TOF} = 180$ ps for Bhabha events. Outside of the time-of-flight counter is a 12-radiation-length barrel shower counter (BSC) comprised of gas proportional tubes interleaved with lead sheets. The BSC measures the energy and direction of photons with resolutions of $\sigma_E/E \simeq 21\%\sqrt{E}$ (E in GeV), $\sigma_\phi = 7.9$ mrad, and $\sigma_z = 2.3$ cm. The iron flux return of the magnet is instrumented with three double layers of counters that are used to identify mouns.

A Geant3 based Monte Carlo (MC) package (SIMBES) with detailed consideration of the detector performance is used. The consistency between data and MC has been carefully checked in many high purity physics channels, and the agreement is reasonable [16]. The detection efficiencies and mass resolutions for each decay mode presented in this paper are obtained with uniform phase space MC generators.

III. ANALYSIS

In this analysis, ω mesons are observed in the $\omega \to \pi^+\pi^-\pi^0$ decay, ϕ mesons in the $\phi \to K^+K^-$ decay, and other mesons are detected in the decays: $K^0_S \to \pi^+\pi^-$, $\pi^0 \to \gamma\gamma$,

$\eta \to \pi^+\pi^-\pi^0$. The final states of the analyzed decays $J/\psi \to \{\omega, \eta\}K^0_S K^\pm\pi^\mp$, $\omega K^+K^-\pi^0$, $\phi K^0_S K^\pm\pi^\mp$, and $\phi K^+K^-\pi^0$ are $2(\pi^+\pi^-)K^\pm\pi^\mp\gamma\gamma$, $\pi^+\pi^-K^+K^-\gamma\gamma\gamma\gamma$, $K^+K^-\pi^+\pi^-K^\pm\pi^\mp$, and $2(K^+K^-)\gamma\gamma$, respectively.

Candidate events are required to satisfy the following common selection criteria:

1. The correct number of charged tracks with net charge zero is required for each event. Each charged track should have a good helix fit in the MDC, and the polar angle θ of each track in the MDC must satisfy $|\cos\theta| < 0.8$. The event must originate from the collision point; tracks except $\pi^\pm$ from K^0_S must satisfy $\sqrt{x^2+y^2} \leq 2$ cm, $|z| \leq 20$ cm, where x, y, and z are the space coordinates of the point of closest approach of tracks to the beam axis.

2. Candidate events should have at least the minimum number of isolated photons associated with the different final states. Each photon should have an energy deposit in the BSC greater than 50 MeV, the angle between the shower development direction and the photon emission direction less than 30°, and the angle between the photon and any charged track larger than 8°.

3. For each charged track in an event, $\chi^2_{PID}(i)$ is determined using both dE/dx and TOF information:
$$\chi^2_{PID}(i) = \chi^2_{dE/dx}(i) + \chi^2_{TOF}(i),$$
where i corresponds to the particle hypothesis. A charged track is identified as a K (π) if χ^2_{PID} for the K (π) hypothesis is less than those for the π and p (K and p) hypotheses.

4. The selected events are subjected to four constraint kinematic fits (4C-fit), unless otherwise specified. When there are more than the minimum number of photons in an event, all combinations are tried, and the combination with the smallest χ^2 is retained.

The branching fraction is calculated using

$$B(J/\psi \to X) = \frac{N_{obs}}{\epsilon_{J/\psi\to X\to Y} \times N_{J/\psi} \times B(X \to Y)}, \quad (1)$$

and the upper limit for a branching fraction is determined using

$$B(J/\psi \to X) < \frac{N_{up}}{\epsilon_{J/\psi\to X\to Y} \times N_{J/\psi} \times B(X \to Y) \times (1-\sigma^{sys})}, \quad (2)$$

where, N_{obs} is the number of events observed, N_{up} is the upper limit on the number of the observed events at the 90% C.L. calculated using a Bayesian method [17], ϵ is the detection efficiency obtained from MC simulation, $N_{J/\psi}$ is the number of J/ψ events, $(5.77\pm0.27)\times10^7$ [18], σ^{sys} is the corresponding systematic error, and $B(X \to Y)$ is the branching fraction, taken from the Particle Data Group (PDG) [17], of the X intermediate state to the Y final state.

A. $J/\psi \to \{\omega, \eta\} K^0_S K^{\pm}\pi^{\mp}$

At least one charged track must be identified as a kaon using TOF and dE/dx information. If there is more than one kaon candidate, the assigned kaon is the one with the largest kaon weight. Candidate events are fitted kinematically using energy momentum conservation (4C-fit) under the $2(\pi^+\pi^-)K^{\pm}\pi^{\mp}\gamma\gamma$ hypothesis, and $\chi^2 < 25$ is required. Each event is required to contain one K^0_S meson with six possible $\pi^+\pi^-$ combinations to test for consistency with the K^0_S. Looping over all combinations, we select the one closest to the K^0_S mass, denoted as $m_{\pi^+\pi^-}$, provided it is within 15 MeV/c^2 of the K^0_S mass. After K^0_S selection, the two remaining oppositely-charged pion combinations along with the two gammas are used to calculate $m_{\pi^+\pi^-\gamma\gamma}$. Figure 1 (a) shows the scatter plot of $m_{\gamma\gamma}$ versus $m_{\pi^+\pi^-\gamma\gamma}$ with two possible entries per event, where clear η and ω signals are seen.

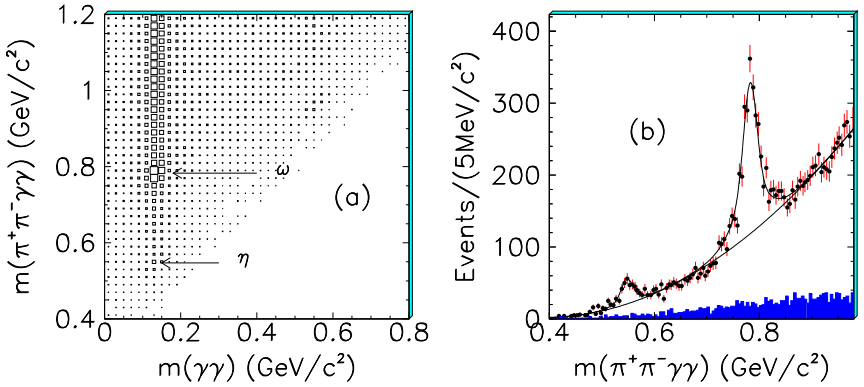

FIG. 1: (a) The scatter plot of $m_{\gamma\gamma}$ versus $m_{\pi^+\pi^-\gamma\gamma}$, and (b) the $\pi^+\pi^-\gamma\gamma$ invariant mass for $J/\psi \to \{\omega, \eta\} K^0_S K^{\pm}\pi^{\mp}$ candidate events with two possible entries per event. The curves in (b) are the results of the fit described in the text, and the shaded histogram in (b) shows the normalized background estimated from the K^0_S-sideband region (0.025 GeV/c^2 $< |m_{\pi^+\pi^-} - m_{K^0_S}| <$ 0.055 GeV/c^2).

The $\pi^+\pi^-\gamma\gamma$ invariant mass distribution with two possible entries per event is shown in Fig. 1 (b), where η and ω signals are apparent. The branching fractions of $J/\psi \to \omega K^0_S K^{\pm}\pi^{\mp}$ and $\eta K^0_S K^{\pm}\pi^{\mp}$ are obtained by fitting this distribution. The backgrounds for $J/\psi \to \omega K^0_S K^{\pm}\pi^{\mp}$ which contribute to the peak in the ω signal region mainly come from non-K^0_S events and events from $J/\psi \to \omega K^0_S K^0_S$ that survive selection criteria. The number of background events from $J/\psi \to \omega K^0_S K^0_S$ is estimated from Monte-Carlo simulation to be less than 2 . Backgrounds for $J/\psi \to \eta K^0_S K^{\pm}\pi^{\mp}$ contributing to the peak in the η signal region mainly come from non-K^0_S events and events from J/ψ decays into $K^{*0}\bar{K}^*_2(1430)^0 \to (K^0_S\pi^0)(K^0_S\eta)$. The latter contribution is estimated to be less than one event from MC simulation. Non-K^0_S events from the K^0_S sideband region (0.025 GeV/c^2 $< |m_{\pi^+\pi^-} - m_{K^0_S}| <$ 0.055 GeV/c^2) are shown in Fig. 1 (b) as the shaded histogram, the background events are 19.2 ± 15.6 ω and -4.1 ± 7.0 η by fitting the distribution with possible signals and polynomial background.

A fit to the $m_{\pi^+\pi^-\gamma\gamma}$ distribution is performed by using ω and η Breit-Wigner (BW) functions folded with Gaussian resolution functions plus a quadratic polynomial, shown

as the curve in Fig. 1 (b). The numbers of events in the ω and η peaks are 1971.7 ± 41.4 and 231.6 ± 23.1, respectively. Here, the background events in the decays of $J/\psi \to \omega K^0_S K^\pm \pi^\mp$ and $J/\psi \to \eta K^0_S K^\pm \pi^\mp$ estimated above are not subtracted but are included in the background systematic error. The $J/\psi \to \omega K^0_S K^\pm \pi^\mp$ and $J/\psi \to \eta K^0_S K^\pm \pi^\mp$ detection efficiencies are obtained from MC simulation to be 1.48% and 1.18%, respectively. The branching fractions are then determined as:

$$B(J/\psi \to \omega K^0_S K^\pm \pi^\mp) \;=\; (3.77 \pm 0.08) \times 10^{-3},$$

$$B(J/\psi \to \eta K^0_S K^\pm \pi^\mp) \;=\; (2.18 \pm 0.22) \times 10^{-3}.$$

Here the errors are statistical only.

1. $J/\psi \to \omega K^* \bar{K} + c.c. \to \omega K^0_S K^\pm \pi^\mp$

To select the ω signal, the mass combination with $\pi^+\pi^-\gamma\gamma$ closest to the ω mass is required to satisfy $|m_{\pi^+\pi^-\gamma\gamma} - m_\omega| < 0.04$ GeV/c^2. Figure 2 shows the scatter plot of $m_{K^0_S\pi}$ versus $m_{K\pi}$ for $J/\psi \to \omega K^0_S K^\pm \pi^\mp$ candidate events, where the events in the cross bands correspond to $J/\psi \to \omega K^* \bar{K} + c.c.$.

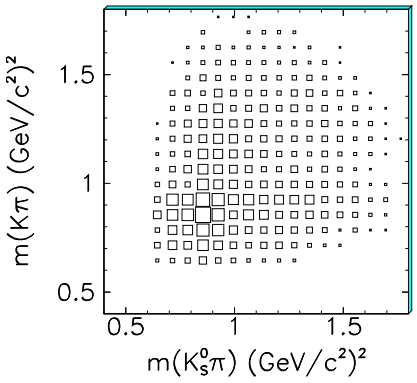

FIG. 2: The scatter plot of $m_{K^0_S\pi}$ versus $m_{K^\pm\pi^\mp}$ for $J/\psi \to \omega K^0_S K^\pm \pi^\mp$ candidate events.

Figure 3 (a) shows the scatter plot of $m_{\pi^+\pi^-\gamma\gamma}$ versus $m_{\pi^+\pi^-}$, and there is an accumulation of events in the ω and K^0_S cross bands. The combined mass spectrum of $K^0_S\pi^\mp$ and $K^\pm\pi^\mp$ in the signal region (box 1 in Fig. 3 (a)), which is defined as $|m_{\pi^+\pi^-} - m_{K^0_S}| < 0.015$ GeV/c^2 and $|m_{\pi^+\pi^-\gamma\gamma} - m_\omega| < 0.04$ GeV/c^2, is shown in Fig. 3 (b), where a clear K^* signal is observed. The K^* signal is fitted with a BW function folded with a Gaussian resolution function plus a third-order polynomial, and 1208.3 ± 93.3 K^* events are obtained.

Non-ω and non-K^0_S backgrounds are studied using ω and K^0_S sideband events. Figure 3 (c) is the fitted $K\pi$ mass spectrum in the ω sideband region ($|m_{\pi^+\pi^-} - m_{K^0_S}| < 0.015$ GeV/c^2, 0.06 GeV/c^2 $< |m_{\pi^+\pi^-\gamma\gamma} - m_\omega| <$ 0.14 GeV/c^2, shown as horizontal sideband boxes 2

in Fig. 3 (a)) and K^0_S sideband region (0.03 GeV/c^2 < $|m_{\pi^+\pi^-} - m_{K^0_S}|$ < 0.06 GeV/c^2, $|m_{\pi^+\pi^-\gamma\gamma} - m_\omega|$ < 0.04 GeV/c^2, shown as vertical sideband boxes 3), and the number of K^* sideband events $N_{sid1} = (686.2 \pm 56.0)$ is obtained. Figure 3 (d) is background from the corner region (0.03 GeV/c^2 < $|m_{\pi^+\pi^-} - m_{K^0_S}|$ < 0.06 GeV/c^2, 0.06 GeV/c^2 < $|m_{\pi^+\pi^-\gamma\gamma} - m_\omega|$ < 0.14 GeV/c^2, shown as diagonal boxes 4), and the number of K^* events N_{sid2} is equal to (134.1 ± 25.5). The number of background events in the signal region is half of the sum of K^* events in the ω sideband and K^0_S sideband regions (N_{sid1}) minus a quarter of the K^* events in the corner regions (N_{sid2}). So $N_{bg} = (686.2 \pm 56.0)/2 - (134.1 \pm 25.5)/4 = (309.6 \pm 28.8)$.

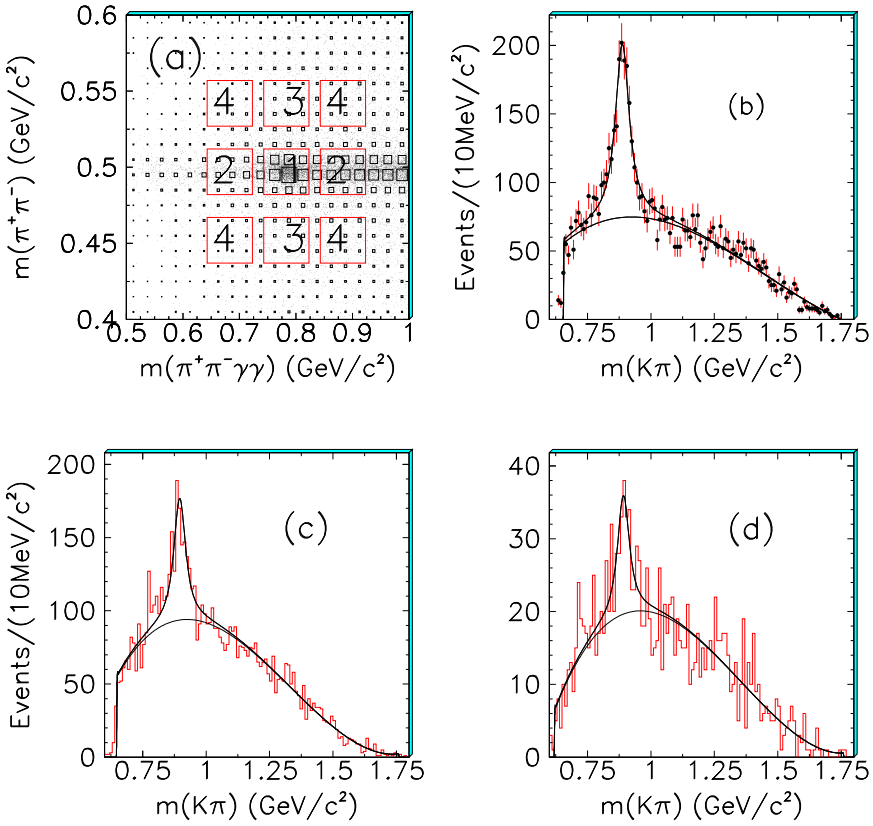

FIG. 3: (a) The scatter plot of $m_{\pi^+\pi^-\gamma\gamma}$ versus $m_{\pi^+\pi^-}$, and the combined mass spectrum of $K^0_S\pi^\mp$ and $K^\pm\pi^\mp$ with two entries per event $J/\psi \to \omega K^* \bar{K} + c.c.$ candidate events for (b) the signal region (the central box 1); (c) the ω and K^0_S sideband regions (two horizontal boxes 2 and two vertical sideband boxes 3); and for (d) the corner region (four diagonal boxes 4). The curves are the results of the fit described in the text.

The detection efficiency is estimated to be 1.23% from MC simulation. After background subtraction, the branching fraction is determined to be

$$B(J/\psi \to \omega K^* \bar{K} + c.c.) \;=\; (6.20 \pm 0.68) \times 10^{-3},$$

where the error is statistical only.

2. $J/\psi \to \omega X(1440) \to \omega K_S^0 K^\pm \pi^\mp$

Figure 4 (a) shows the scatter plot of $m_{K_S^0 K^\pm \pi^\mp}$ versus $m_{\pi^+\pi^-\gamma\gamma}$, and Fig. 4 (b) is the $K_S^0 K^\pm \pi^\mp$ invariant mass spectrum after ω selection ($|m_{\pi^+\pi^-\gamma\gamma} - m_\omega| < 0.04$ GeV/c^2). Figs. 4 (a) and (b) show a resonance near 1.44 GeV/c^2, denoted as $X(1440)$. To ensure that this peak is not due to background, we have made studies of potential background processes using both data and MC simulations. Non-ω and non-K_S^0 processes are studied with ω and K_S^0 mass sideband events, respectively. The main background channel $J/\psi \to \omega 2(\pi^+\pi^-)$ and other background processes with 6-prong events are studied by MC simulation. In addition, we also checked for possible backgrounds with a MC sample of 60×10^6 $J/\psi \to$ *anything* decays generated by the LUND-charm model [19]. None of these background sources produces a peak around 1.44 GeV/c^2 in the $K_S^0 K^\pm \pi^\mp$ invariant mass spectrum.

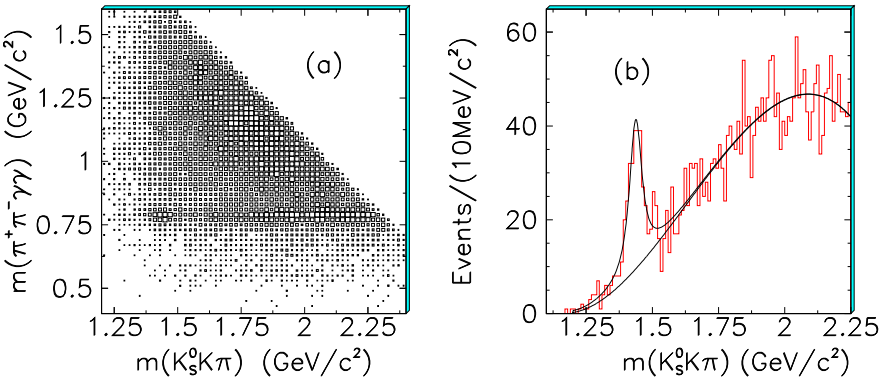

FIG. 4: (a) The scatter plot of $m_{K_S^0 K^\pm \pi^\mp}$ versus $m_{\pi^+\pi^-\gamma\gamma}$ and (b) the $K_S^0 K^\pm \pi^\mp$ invariant mass distribution for $J/\psi \to \omega K_S^0 K^\pm \pi^\mp$ candidate events. The curves in (b) are the results of the fit described in the text.

The $K_S^0 K^\pm \pi^\mp$ invariant mass distribution is fitted with a BW function convoluted with a Gaussian mass resolution function ($\sigma = 7.44$ MeV/c^2) to represent the $X(1440)$ signal and a third-order polynomial background function. The mass and width obtained from the fit are $M = 1437.6 \pm 3.2$ MeV/c^2 and $\Gamma = 48.9 \pm 9.0$ MeV/c^2, and the fit yields 248.8 ± 35.2 events.

Using the efficiency of 1.45% determined from a uniform phase space MC simulation, we obtain the branching fraction to be

$$B(J/\psi \to \omega X(1440)) \cdot B(X(1440) \to K_S^0 K^\pm \pi^\mp) \;=\; (4.86 \pm 0.69) \times 10^{-4},$$

where the error is only the statistical error.

B. $J/\psi \to \omega K^+ K^- \pi^0$

At least one charged track is required to be a kaon and the combined PID probability for $K^+K^-\pi^+\pi^-$ is required to be greater than those for the $K^\pm\pi^\mp\pi^+\pi^-$ and $\pi^+\pi^-\pi^+\pi^-$

hypotheses. A 4C kinematic fit is made under the $K^+K^-\pi^+\pi^-4\gamma$ hypothesis. There are three combinations to form two π^0's, and further a six-constraint kinematic fit (6C-fit) with the smallest χ^2_{6C} is made requiring two π^0's from four photons. Events with $\chi^2_{4C} < 50$ and $\chi^2_{6C} < 50$ are selected. To reject the possible multiple photon background events, χ^2_{4C} is required to be less than those for the $K^+K^-\pi^+\pi^-2\gamma$, $K^+K^-\pi^+\pi^-3\gamma$, and $K^+K^-\pi^+\pi^-5\gamma$ hypotheses. Background events with K^0_S decays, such as $K^{*0}\bar{K}^*_2(1430)^0 \to K^0_S K^\pm\pi^\mp\{\pi^0, 2\pi^0\}$, and $\gamma K^*\bar{K}^* \to \gamma K^0_S K^\pm\pi^\mp\pi^0$, are eliminated by requiring $|m_{\pi^+\pi^-} - m_{K^0_S}| > 0.02$ GeV/c^2 in the $\pi^+\pi^-$ invariant mass.

There are two $\pi^+\pi^-\pi^0$ mass combinations, and the one closest to the ω mass, denoted as $m_{\pi^+\pi^-\pi^0}$, is selected. The scatter plot of $m_{K^+K^-\pi^0}$ versus $m_{\pi^+\pi^-\pi^0}$ is shown in Fig. 5 (a), where the circle indicates some enhancement from $J/\psi \to \omega X(1440)$ events in the $\omega K^+K^-\pi^0$ decay.

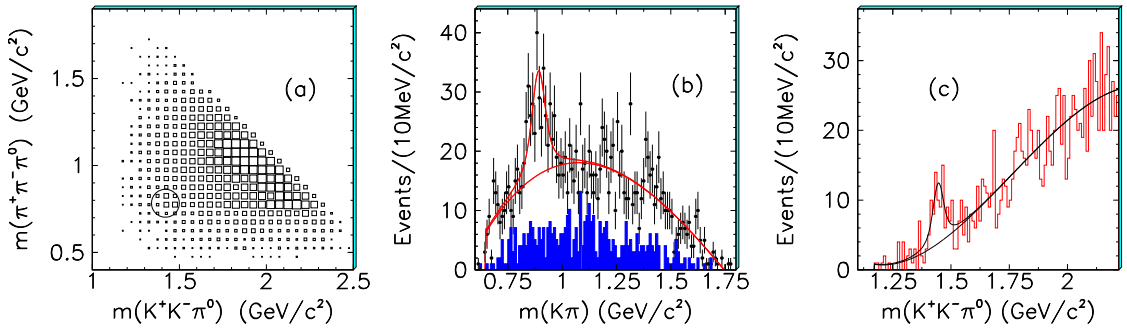

FIG. 5: (a) The scatter plot of $m_{K^+K^-\pi^0}$ versus $m_{\pi^+\pi^-\pi^0}$, (b) the $K^\pm\pi^0$ invariant mass distribution with two possible entries per event, and (c) the $K^+K^-\pi^0$ invariant mass distribution for $J/\psi \to \pi^+\pi^-\pi^0K^+K^-\pi^0$ candidate events. The curves are the results of the fit described in the text, and the shaded histogram (b) shows the normalized background estimated from the ω-sideband region.

1. $J/\psi \to \omega K^{*\pm}K^\mp \to \omega K^+K^-\pi^0$

To suppress the main K^{*0} backgrounds, $|m_{K^\pm\pi^\mp} - m_{K^{*0}}| > 0.05$ GeV/c^2 is required. In addition to the above selection, the further requirement of $|m_{\pi^+\pi^-\pi^0} - m_\omega| < 0.04$ GeV/c^2 is imposed. The combined mass spectrum of $K^+\pi^0$ and $K^-\pi^0$ is shown in Fig. 5 (b), where the $K^{*\pm}$ signal is seen, and is fitted to obtain the branching fraction of $J/\psi \to \omega K^{*\pm}K^\mp$.

Background events for $\omega K^{*\pm}K^\mp$ which could contribute to the peak in the $K^{*\pm}$ signal region mainly come from events with K^* decays, such as $J/\psi \to K^{*0}\bar{K}^*_2(1430)^0$ into 4-prong plus multiple photons, $J/\psi \to \phi K^*\bar{K}$, and $J/\psi \to \gamma K^*\bar{K}^*$, but their contributions can be ignored according to MC studies. It is further confirmed that the $J/\psi \to \omega K^{*\pm}K^\mp$ background is negligible using ω and π^0 sideband events.

The $K^\pm\pi^0$ invariant mass distribution in Fig. 5 (b) (2 entries/event) is fitted with a $K^{*\pm}$ BW function with the mass and width fixed to PDG values [17] plus a third-order polynomial. The number of $K^{*\pm}$ events obtained is (175.6 ± 27.4). The detection efficiency is 0.32%, and the branching fraction of $J/\psi \to \omega K^*\bar{K} + c.c.$ is determined to be

$$B(J/\psi \to \omega K^* \bar{K} + c.c.) \;=\; (6.53 \pm 1.02) \times 10^{-3},$$

where the error is statistical only.

2. $J/\psi \to \omega X(1440) \to \omega K^+ K^- \pi^0$

Figure 5 (c) shows the $K^+K^-\pi^0$ invariant mass recoiling against the ω, where a $X(1440)$ signal is observed. We have also studied potential background processes using both data and MC simulations. Non-ω processes are studied with the ω mass sideband events (0.06 GeV/c^2 $< |m_{\pi^+\pi^-\pi^0} - m_\omega| <$ 0.10 GeV/c^2). Background with ω decays is studied by MC simulations, similar to those of $J/\psi \to \omega K^* \bar{K} + c.c. \to \omega K^+ K^- \pi^0$. In addition, we also checked for possible backgrounds using a MC sample of 60×10^6 $J/\psi \to$ *anything* decays generated by the LUND-charm model. In each case, the $K^+K^-\pi^0$ mass distribution shows no evidence of an enhancement near 1440 MeV/c^2.

By fitting the $K^+K^-\pi^0$ mass spectrum in Fig. 5 (c) with a BW function convoluted with a Gaussian mass resolution function ($\sigma = 14.2$ MeV/c^2) plus a third-order polynomial background function, the mass and width of $M = 1445.9 \pm 5.7$ MeV/c^2 and $\Gamma = 34.2 \pm 18.5$ MeV/c^2 are obtained, and the number of events from the fit is 62.1 ± 18.3. A fit without a BW signal function returns a value of $-2 \ln L$ larger than the nominal fit by 31.7 with three degrees of freedom (d.o.f.), corresponding to a statistical significance of 5.0 σ for the signal.

The efficiency is determined to be 0.64% from a phase space MC simulation, and the branching fraction is

$$B(J/\psi \to \omega X(1440)) \cdot B(X(1440) \to K^+K^-\pi^0) \;=\; (1.92 \pm 0.57) \times 10^{-4},$$

where the error is statistical.

C. $J/\psi \to \phi K^0_S K^\pm \pi^\mp$

Events with six charged tracks are selected, and at least two charged tracks must be identified as kaons. If there are more than two kaons, the two kaons with the largest kaon PID probabilities are regarded as the real kaons. The other charged tracks are assumed, one at a time, to be a kaon, while the other three to be pions, and these combinations of three kaons and three pions are kinematically fitted. The hypothesis with the smallest χ^2 is considered as the right combination, and $\chi^2 < 20$ is required. Two combinations of oppositely charged pions are used to reconstruct the K^0_S signal, and the one closest to the K^0_S mass is required to be within 15 MeV/c^2.

The invariant mass of the two mass combinations formed with oppositely charged kaons are shown in Fig. 6, where a clear ϕ signal is observed. A fit to the K^+K^- mass distribution in Fig 6 is performed to obtain the number of $J/\psi \to \phi K^0_S K^\pm \pi^\mp$ events. Backgrounds contributing to the ϕ signal peak mainly come from J/ψ into $\phi f_2'(1525) \to \phi\eta\eta$, $\phi\eta' \to \phi\eta\pi^+\pi^-$, $\phi K^0_S K^0_S$, and $\phi 2(\pi^+\pi^-)$ (excluding $\phi K^0_S K^0_S$). From MC simulations of these

background channels, the number of background ϕ events in the signal region is less than one, and K^0_S-sideband events also show that the background is negligible.

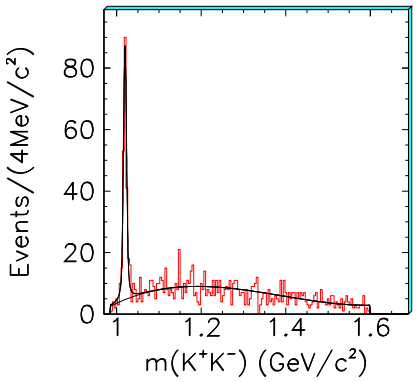

FIG. 6: The K^+K^- invariant mass distribution for $J/\psi \to K^+K^-\pi^+\pi^-K^\pm\pi^\mp$ candidate events with two possible entries per event. The curves are the results of the fit described in the text.

The K^+K^- mass distribution in Fig. 6 is fitted with a BW function convoluted with a Gaussian mass resolution function ($\sigma = 2.93$ MeV/c^2) plus a third-order polynomial background function. The number of ϕ events from the fit is 227.1 ± 19.0. Using the detection efficiency of 1.56%, the corresponding branching fraction is

$$B(J/\psi \to \phi K^0_S K^\pm \pi^\mp) \;=\; (7.37 \pm 0.62) \times 10^{-4},$$

where the error is statistical only.

1. $J/\psi \to \phi K^* \bar{K} + c.c. \to \phi K^0_S K^\pm \pi^\mp$

To remove most non-ϕ background events, the K^+K^- combination closest to the ϕ mass is required to satisfy $|m_{K^+K^-} - m_\phi| < 0.015$ GeV/c^2. The scatter plot of $m_{K^0_S\pi}$ versus $m_{K\pi}$ for candidate events is shown in Fig. 7 (a), where the events in the cross band correspond to the K^* signal.

The scatter plot of $m_{\pi^+\pi^-}$ versus $m_{K^+K^-}$ is shown in Figure 7 (b), and there is an accumulation of events in the ϕ and K^0_S cross bands. Figure 7 (c) shows the combined $K^0_S\pi^\mp$ and $K^\pm\pi^\mp$ mass spectrum for events in the signal region (box 1 in Fig. 7 (b)), which is defined as $|m_{\pi^+\pi^-} - m_{K^0_S}| < 0.015$ GeV/c^2 and $|m_{K^+K^-} - m_\phi| < 0.015$ GeV/c^2. A fit yields 194.8 ± 25.0 K^* events.

The same method as used for the $J/\psi \to \omega K^* \bar{K} + c.c. \to \omega K^0_S K^\pm \pi^\mp$ analysis is used to estimate the number of background events in the signal region, and $N_{bg} = (10.0 \pm 6.6)$, which is neglected in the branching fraction determination.

The detection efficiency of $J/\psi \to \phi K^* \bar{K} + c.c.$ in this decay is 1.42%, and its branching fraction is determined to be

$$B(J/\psi \to \phi K^* \bar{K} + c.c.) \;=\; (2.08 \pm 0.27) \times 10^{-3},$$

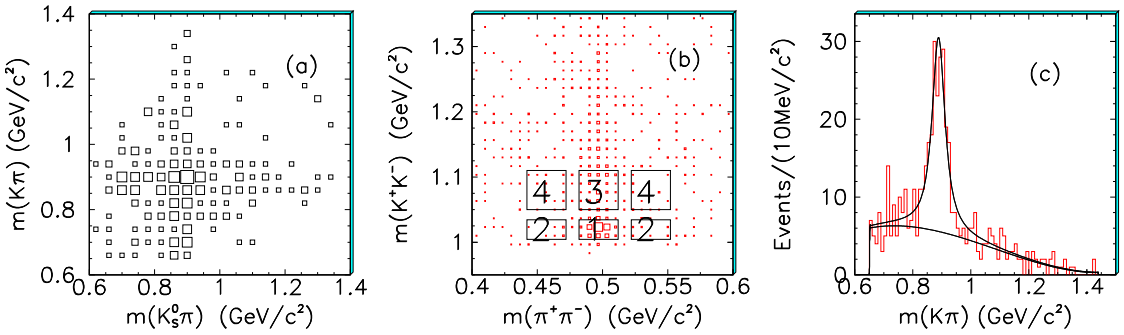

FIG. 7: (a) The scatter plot of $m_{K^0_S\pi}$ versus $m_{K\pi}$, (b) the scatter plot of $m_{\pi^+\pi^-}$ versus $m_{K^+K^-}$, and (c) the combined $K^0_S\pi^\mp$ and $K^\pm\pi^\mp$ invariant mass distributions for events in the signal region (box 1) for $J/\psi \to \phi K^0_S K^\pm\pi^\mp$ candidate events. The curves are the results of the fit described in the text.

where the error is statistical only.

2. $J/\psi \to \phi X(1440) \to \phi K^0_S K^\pm\pi^\mp$

The distribution of $K^0_S K^\pm\pi^\mp$ invariant mass recoiling against the ϕ signal is shown in Fig. 8 (a), and there is no evidence for $X(1440)$. The upper limit on the number of the observed events at the 90% C.L. is 8.1 [17]. The likelihood distribution and the 90% C.L. limit are shown in Fig. 8 (b). The likelihood values for the number of events are obtained by fitting the $K^0_S K^\pm\pi^\mp$ distributions with a X(1440) signal plus a third-order polynomial background. Its mass and width are fixed to those in the decay $J/\psi \to \omega X(1440) \to \omega K^0_S K^\pm\pi^\mp$.

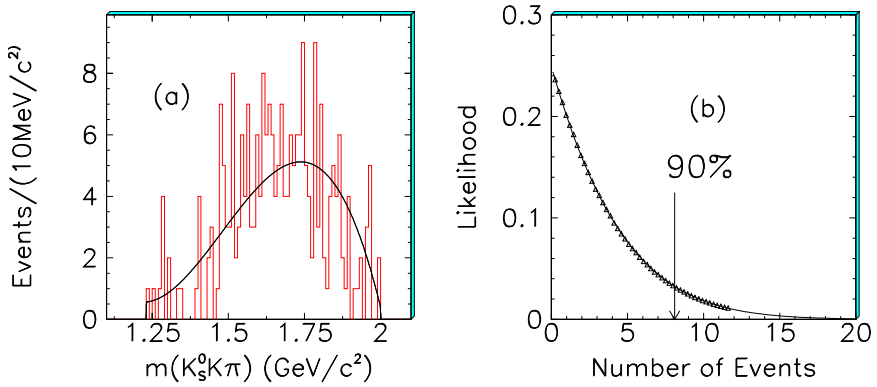

FIG. 8: (a) The $K^0_S K^\pm\pi^\mp$ invariant mass recoiling against the ϕ, and (b) the number of events of X(1440). The curve in (a) is a third order polynomial to describe the background, and the observed number of events at the 90% confidence level using a Bayesian method is indicated by the arrow in (b).

The detection efficiency is 2.53%, and the upper limit on the branching fraction at the

90% C.L. is:

$$B(J/\psi \to \phi X(1440) \to \phi K_S^0 K^+\pi^- + c.c.) < 1.93 \times 10^{-5}. \quad (3)$$

D. $J/\psi \to \phi K^+K^-\pi^0$

At least three charged tracks must be identified as kaons. A 4C-fit is applied under the hypothesis $J/\psi \to \gamma\gamma 2(K^+K^-)$, and $\chi^2 < 16$ is required. To reject possible background events from $J/\psi \to \gamma 2(K^+K^-)$, the χ^2 of the 4C fit for $J/\psi \to \gamma\gamma 2(K^+K^-)$ is required to be less than that for the $\gamma 2(K^+K^-)$ hypothesis. There are four possible ways to combine the oppositely charged kaons in forming the ϕ, and the K^+K^- combination closest to the ϕ mass is chosen. Figure 9 (a) shows the scatter plot of $m_{\gamma\gamma}$ versus $m_{K^+K^-}$, and clear ϕ and π^0 signals are seen.

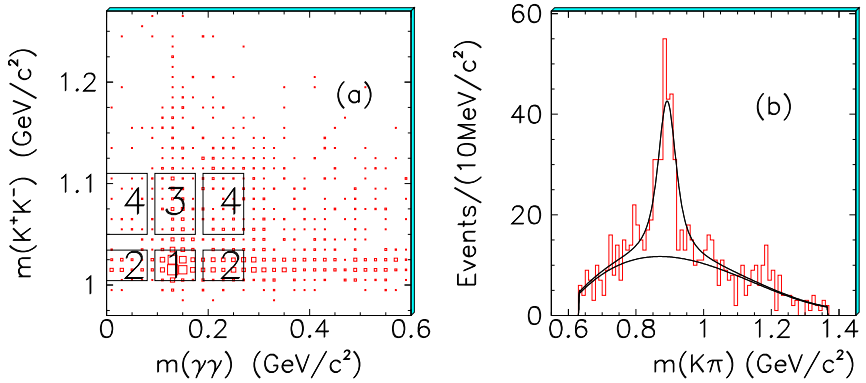

FIG. 9: (a) The scatter plot of $m_{\gamma\gamma}$ versus $m_{K^+K^-}$, and (b) the $K^\pm\pi^0$ invariant mass distribution for events in the signal region (box 1) for $J/\psi \to \gamma\gamma 2(K^+K^-)$ candidate events with two entries per event. The curves are the results of the fit described in the text.

1. $J/\psi \to \phi K^{*\pm}K^\mp \to \phi K^+K^-\pi^0$

Figure 9 (b) shows the $K^\pm\pi^0$ combined mass spectrum for events in the signal region (box 1 in Fig. 9 (a)), which is defined as $|m_{K^+K^-} - m_\phi| < 0.015$ GeV/c^2 and $|m_{\gamma\gamma} - m_{\pi^0}| < 0.04$ GeV/c^2, and a clear $K^{*\pm}$ signal is seen. It is fitted with a BW, whose mass and width are fixed to those of $K^{*\pm}$ in the PDG, plus a third-order polynomial. The number of $K^{*\pm}$ events from the fit is 277.8 ± 27.7. The sidebands are used as before to estimate the number of the corresponding background events in the signal region, and the result is $N_{bg} = (40.1 \pm 10.1)$.

After subtracting the above background and incorporating the efficiency of 1.71% from MC simulation, the branching fraction is determined to be

$$B(J/\psi \to \phi K^* \bar{K} + c.c.) \;=\; (2.96 \pm 0.37) \times 10^{-3},$$

where the error is statistical only.

2. $J/\psi \to \phi X(1440) \to \phi K^+K^-\pi^0$

The distribution of $K^+K^-\pi^0$ invariant mass recoiling against the ϕ is shown in Fig. 10 (a). No evidence for the $X(1440)$ is observed near 1440 MeV/c^2. The upper limit on the number of the observed events at the 90% C.L. is 10.5 [17]. The likelihood distribution and the 90% C.L. limit are shown in Fig. 10 (b). The likelihood values for the number of events are obtained by fitting the $K^+K^-\pi^0$ distributions with a X(1440) signal, whose mass and width are fixed to those of the decay $J/\psi \to \omega K^+K^-\pi^0$, plus a third-order background polynomial. The detection efficiency is 2.49%, and the upper limit on the branching fraction at the 90% C.L. is:

$$B(J/\psi \to \phi X(1440) \to \phi K^+K^-\pi^0) < 1.71 \times 10^{-5}. \quad (4)$$

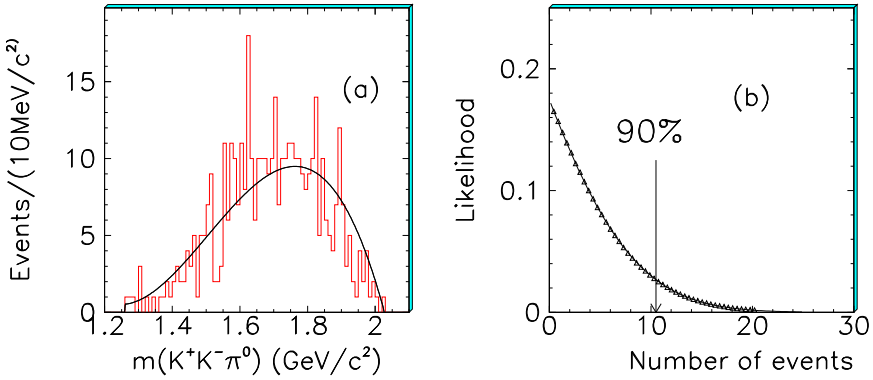

FIG. 10: (a) The $K^+K^-\pi^0$ invariant mass recoiling against the ϕ, and (b) the number of events of X(1440). The curve in (a) is the third-order polynomial to describe the background, and the observed number of events at the 90% confidence level using a Bayesian method is indicated by arrow in (b).

IV. SYSTEMATIC ERRORS

In this analysis, the systematic errors on the branching fractions mainly come from following sources:

- MDC tracking efficiency

  The MDC tracking efficiency is measured from clean channels like $J/\psi \to \Lambda\bar{\Lambda}$ and $\psi(2S) \to \pi^+\pi^- J/\psi$ with $J/\psi \to \mu^+\mu^-$. It is found that the MC simulation agrees with data within $1\% - 2\%$ for each charged track. Therefore, 12% is taken as the systematic error on the tracking efficiency for the channels with six charged tracks and 8% for the channels with four charged tracks in the final states.

- Photon detection efficiency

  The photon detection efficiency is studied from $J/\psi \to \rho^0\pi^0$ events [20]. The results indicate that the difference between data and MC simulation is less than 2% for each photon. Therefore, 4% is taken to be the systematic error from the photon efficiency for the channels with two photons and 8% for the channels with four photons in the final states.

- PID

  The PID efficiency of the kaon is studied with $J/\psi \to K^+K^-\pi^0$ events. The average PID efficiency difference between data and MC is found to be less than 2%. In this paper, 2%, 4%, and 6% are conservatively taken as the systematic errors on PID efficiency for the channels with one, two, and three identified kaons, respectively.

- K^0_S reconstruction

  The K^0_S secondary vertex reconstruction is checked using $J/\psi \to K^{*\pm}K^{\mp}(K^{*\pm} \to K^0_S\pi^{\pm})$ events. It is found that the difference of the efficiency between data and MC simulation is 2.8%, which is taken to be the systematic error from the K^0_S secondary vertex reconstruction.

- Intermediate decay branching fractions

  The branching fractions for $\eta \to \pi^+\pi^-\pi^0$, $\omega \to \pi^+\pi^-\pi^0$, and $\phi \to K^+K^-$ are taken from the PDG [17], and the errors on these branching fractions are included as systematic errors in our measurements. The error on the $K^0_S \to \pi^+\pi^-$ branching fraction is neglected in this analysis.

- Kinematic fit

  Kinematic fits are used to reduce backgrounds. Using the same method as in Ref. [21], the decay modes $J/\psi \to 3(\pi^+\pi^-)\pi^0$, $J/\psi \to 2(\pi^+\pi^-)\pi^0$, and $J/\psi \to 3(\pi^+\pi^-)$ are studied [22] in order to estimate the corresponding systematic error. The kinematic fit efficiency differences between data and MC are 5.5%, 4.3%, and 8.7%, respectively. The efficiency difference between data and MC for the 6C-kinematic fit to $\eta_C \to \omega\omega \to 2(\pi^+\pi^-\pi^0)$ is about 10% [23]. Since the decays in this analysis are similar to the above decays, these systematic errors are taken as the corresponding systematic errors.

- Background uncertainty

TABLE I: Systematic errors in $B(J/\psi \to \{\eta, \omega, \phi\}K\bar{K}\pi)$.

$J/\psi \to$	$\eta K_S^0 K^\pm \pi^\mp$	$\omega K_S^0 K^\pm \pi^\mp$	$\omega K^* K \to$ $\omega K_S^0 K^\pm \pi^\mp$	$\omega K^* K \to$ $\omega K^+ K^- \pi^0$	$\phi K_S^0 K^\pm \pi^\mp$	$\phi K^* K \to$ $\phi K_S^0 K^\pm \pi^\mp$	$\phi K^* K \to$ $\phi K^+ K^- \pi^0$
Error source	relative error (%)						
MDC tracking	12	12	12	8	12	12	8
photon efficiency	4	4	4	8	-	-	4
Particle ID	2	2	2	2	4	4	6
K_S^0 2nd vertex	2.8	2.8	2.8	-	2.8	2.8	-
intermediate decays	1.8	0.8	0.8	0.8	1.2	1.2	1.2
kinematic fit	5.5	5.5	5.5	10	8.2	8.2	4.3
Back. uncertainty	1.8	2.0	5.9	11.7	8.4	6.1	7.3
MC statistic	1.9	1.3	2.3	3.2	3.2	3.4	2.2
MC model	-	-	5.1	5.1	-	5.1	5.1
Number of J/ψ events	4.7						
total Sum	15.4	15.2	17.1	20.7	18.4	18.3	15.6

The background uncertainties come from the uncertainties associated with the estimation of the sideband backgrounds, the events from other background channels, as well as the uncertainties of background shapes, different fit ranges, and different binning. Therefore, the statistical error in the estimated number of background events, the largest difference from changing background shape, the difference from changing the fit range, the difference of changing fit binning, and some ignored backgrounds events are taken as the systematic errors due to the background uncertainty.

- MC generator

  There may be interference between charged and neutral K^* modes, which is not included in the MC generator. In the sample of $J/\psi \to \omega K^* \bar{K} + c.c. \to \omega K_S^0 K^\pm \pi^\mp$ decays, the $K^\pm \pi^\mp$ mass distribution in the $K^{*\pm}$ sideband and signal regions and the $K_S^0 \pi$ mass distributions in the K^{*0} sideband and signal regions from the scatter plot of $m_{K^\pm \pi^\mp}$ versus $m_{K_S^0 \pi^\mp}$, are studied in real data and MC simulation. It is found that the difference between data and MC sample is 5.1%, so 5.1% is taken as the systematic error from the MC model.

- Number of J/ψ events

  The number of J/ψ is $(57.7 \pm 2.7) \times 10^6$, determined from J/ψ inclusive four-prong events [18]. The uncertainty is taken as a systematic error in the branching ratio measurement.

Table I and Table II list the systematic errors from all above sources, and the total systematic error is the sum of them added in quadrature.

TABLE II: Systematic errors in $B(J/\psi \to \{\omega,\phi\}X(1440) \to \{\omega,\phi\}K\bar{K}\pi)$.

$J/\psi \to$	$\omega X(1440)$ $\to \omega K^0_S K^\pm \pi^\mp$	$\omega X(1440)$ $\to \omega K^+ K^- \pi^0$	$\phi X(1440)$ $\to \phi K^0_S K^\pm \pi^\mp$	$\phi X(1440)$ $\to \phi K^+ K^- \pi^0$
Error source	relative error (%)			
MDC tracking	12	8	12	8
photon efficiency	4	8	-	4
Particle ID	2	2	4	6
K^0_S 2nd vertex	2.8	-	2.8	-
intermediate decays	0.8	0.8	1.3	1.2
kinematic fit	5.5	10	8.2	4.3
MC statistic	2.7	2.6	0.8	0.8
Back. uncertainty	6.4	10.9	-	-
Number of J/ψ events	4.7			
Sum	16.6	19.6	16.2	12.6

TABLE III: The branching fractions of J/ψ decays in BESII.

Decay	final state	No. of events	efficiency	Branching fraction (10^{-4})
$\omega K^0_S K^+\pi^- + c.c.$	$(\pi^+\pi^-\pi^0)K^0_S K^\pm\pi^\mp$	1971.7 ± 41.4	1.48%	$37.7 \pm 0.8 \pm 5.8$
$\eta K^0_S K^+\pi^- + c.c.$	$(\pi^+\pi^-\pi^0)K^0_S K^\pm\pi^\mp$	231.6 ± 23.1	1.18%	$21.8 \pm 2.2 \pm 3.4$
$\omega K^*\bar{K} + c.c.$	$(\pi^+\pi^-\pi^0)K^0_S K^\pm\pi^\mp$	898.7 ± 97.7	1.23%	$62.0 \pm 6.8 \pm 10.6$
	$(\pi^+\pi^-\pi^0)K^+K^-\pi^0$	175.6 ± 27.4	0.32%	$65.3 \pm 10.2 \pm 13.5$
$\phi K^0_S K^+\pi^- + c.c.$	$(K^+K^-)K^0_S K^\pm\pi^\mp$	227.1 ± 19.0	1.56%	$7.4 \pm 0.6 \pm 1.4$
$\phi K^*\bar{K} + c.c.$	$(K^+K^-)K^0_S K^\pm\pi^\mp$	194.8 ± 25.0	1.42%	$20.8 \pm 2.7 \pm 3.9$
	$(K^+K^-)K^+K^-\pi^0$	237.7 ± 29.5	1.71%	$29.6 \pm 3.7 \pm 4.7$

V. RESULTS

Table III lists the branching fractions of $J/\psi \to \{\eta,\omega,\phi\}K^0_S K^\pm\pi^\mp$, $J/\psi \to \{\omega,\phi\}K^*\bar{K} + c.c.$ from different decay modes. These branching fractions are somewhat larger than those of other experiments in Table IV [24] [25] but they are still consistent within errors. The branching fraction for $J/\psi \to \eta K^0_S K^\pm\pi^\mp$ is measured for the first time. In the invariant mass spectra of $K^0_S K^\pm\pi^\mp$ and $K^+K^-\pi^0$ recoiling against the ω, the resonance at 1.44 GeV/c^2 is observed, with the mass, width, and branching fractions listed in Table V; while in the invariant mass spectra of $K^0_S K^\pm\pi^\mp$ and $K^+K^-\pi^0$ recoiling against the ϕ, no significant structure near 1.44 GeV/c^2 is seen and an upper limits on the J/ψ decay branching fractions at the 90% C.L. are given in Table V.

Acknowledgments

The BES collaboration thanks the staff of BEPC and computing center for their hard efforts. This work is supported in part by the National Natural Science Foundation of China under contracts Nos. 10491300, 10225524, 10225525, 10425523, 10625524, 10521003,

TABLE IV: The branching fractions of J/ψ decays from MarkIII [24] and DM2 [25] Collaborations

	Decay	final state	Branching fraction (10^{-4})
MarkIII	$\omega K_S^0 K^+\pi^- + c.c.$	$(\pi^+\pi^-\pi^0)K_S^0 K^\pm\pi^\mp$	$29.5 \pm 1.4 \pm 7.0$
	$\omega K^*\bar{K} + c.c.$	$(\pi^+\pi^-\pi^0)K_S^0 K^\pm\pi^\mp$ $(\pi^+\pi^-\pi^0)K^+K^-\pi^0$	$53 \pm 14 \pm 14$
	$\phi K_S^0 K^+\pi^- + c.c.$	$(K_S^0 K_L^0))K_S^0 K^\pm\pi^\mp$ $(K^+K^-)K_S^0 K^+\pi^- + c.c.$	$7.0 \pm 0.6 \pm 1.0$
DM2	$\phi K_S^0 K^+\pi^- + c.c.$	$(K^+K^-)K_S^0 K^\pm\pi^\mp$	$7.4 \pm 0.9 \pm 1.1$
	$\phi K^*\bar{K} + c.c.$	$(K^+K^-)K_S^0 K^\pm\pi^\mp$	$20.8 \pm 2.7 \pm 3.7$

TABLE V: The mass, width, and branching fractions of J/ψ decays into $\{\omega, \phi\}X(1440)$.

$J/\psi \to \omega X(1440)$ $(X \to K_S^0 K^+\pi^- + c.c.)$	$J/\psi \to \omega X(1440)$ $(X \to K^+K^-\pi^0)$
$M = 1437.6 \pm 3.2$ MeV/c^2	$M = 1445.9 \pm 5.7$ MeV/c^2
$\Gamma = 48.9 \pm 9.0$ MeV/c^2	$\Gamma = 34.2 \pm 18.5$ MeV/c^2
$B(J/\psi \to \omega X(1440) \to \omega K_S^0 K^+\pi^- + c.c.) = (4.86 \pm 0.69 \pm 0.81) \times 10^{-4}$	
$B(J/\psi \to \omega X(1440) \to \omega K^+K^-\pi^0) = (1.92 \pm 0.57 \pm 0.38) \times 10^{-4}$	
$B(J/\psi \to \phi X(1440) \to \phi K_S^0 K^+\pi^- + c.c.) < 1.93 \times 10^{-5}$ (90% C.L.)	
$B(J/\psi \to \phi X(1440) \to \phi K^+K^-\pi^0) < 1.71 \times 10^{-5}$ (90% C.L.)	

the Chinese Academy of Sciences under contract No. KJ 95T-03, the 100 Talents Program of CAS under Contract Nos. U-11, U-24, U-25, and the Knowledge Innovation Project of CAS under Contract Nos. U-602, U-34 (IHEP), the National Natural Science Foundation of China under Contract No. 10225522 (Tsinghua University), and the Department of Energy under Contract No. DE-FG02-04ER41291 (U. Hawaii).

[1] P. H. Baillon *et al.*, NC 50A, 393 (1967).
[2] D. L. Scharre *et al.*, Phys. Lett. B **97**, 329 (1980).
[3] C. Edwards *et al.*, Phys. Rev. Lett. **49**, 259 (1982); Phys. Rev. Lett. **50**, 219 (1982).
[4] J. E. Augustin *et al.* (DM2 Collaboration), Phys. Rev. D **42**, 10 (1990).
[5] M. G. Rath *et al.*, Phys. Rev. D **40**, 693 (1989).
[6] T. Adams *et al.*, Phys. Rev. Lett. **87**, 041801 (2001).
[7] Z. Bai *et al.* (MarkIII Collaboration), Phys. Rev. Lett. **65**, 2507 (1990).
[8] J. E. Augustin *et al.* (DM2 Collaboration), Phys. Rev. D **46**, 1951 (1992).
[9] A Bertin *et al.* (OBELIX Collaboration), Phys. Lett. B **361**, 187 (1997); Phys. Lett. B **400**, 226 (1997).
[10] C. Cicalo *et al.* (OBELIX Collaboration), Phys. Lett. B **462**, 453 (1999).
[11] F. Nichitiu *et al.* (OBELIX Collaboration), Phys. Lett. B **545**, 261 (2002).
[12] T. Bolton *et al.*, Phys. Rev. Lett. **69**, 1328 (1992).
[13] C. Amsler *et al.* (Crystal Barrel Collaboration), Phys. Lett. B **358**, 389 (1995).
[14] M. Acciarri *et al.* (L3 Collaboration), Phys. Lett. B **501**, 1 (2001).

[15] J. Z. Bai *et al.* (BES Collaboration), Nucl. Instrum. and Meth. A **458**, 627 (2001).
[16] M. Ablikim *et al.* (BES Collaboration), Nucl. Instrum. and Meth. A **552**, 344 (2005).
[17] W. M. Yao *et al.* (Particle Data Group), J. Phys. G **33**, 1 (2006).
[18] S. S. Fang *et al.*, High Energy Phys. Nucl. Phys. **27**, 277 (2003).
[19] J. C. Chen *et al.*, Phys. Rev. D **62**, 034003 (2000).
[20] S. M. Li *et al.*, High Energy Phys. Nucl. Phys. **28**, 859 (2004).
[21] J. Z. Bai *et al.* (BES Collaboration), Phys. Rev. D **70**, 012005 (2004).
[22] M. Ablikim *et al.* (BES Collaboration), Phys. Lett. B **610**, 192 (2005).
[23] M. Ablikim *et al.* (BES Collaboration), Phys. Rev. D **72**, 072005 (2005).
[24] J. Becker *et al.* (MarkIII Collaboration), Phys. Rev. Lett. **59**, 186 (1987).
[25] A. Falvard *et al.* (DM2 Collaboration), Phys. Rev. D **38**, 2706 (1988).